Liang, X., Tian, X., Zhu, G., Wu, C., Duan, Y., Li, W., Zhou, B., Zhang, M., Yu, G., Nie, S., Wang, G., Wang, M., Wu, Z., Liu, Z., Guo, X., Zhou, X., Wei, Z., Xu, T., Zhang, X., Bai, Z., Chen, Y., Teng, J., 2016. SANDWICH: A 2D Broadband Seismic Array in Central Tibet. *Seismological Research Letters*, 87(4), 864-873.

SANDWICH: A 2D Broadband Seismic Array in Central Tibet

by Xiaofeng Liang, Xiaobo Tian, Gaohua Zhu, Chenglong Wu, Yaohui Duan, Wei Li, Beibei Zhou, Minghui Zhang, Guiping Yu, Shitan Nie, Gaochun Wang, Minling Wang, Zhenbo Wu, Zhen Liu, Xi Guo, Xiaopeng Zhou, Zhi Wei, Tao Xu, Xi Zhang, Zhiming Bai, Yun Chen, and Jiwen Teng

ABSTRACT

The tectonic processes that formed the Tibetan plateau have been a significant topic in earth science, but images of the subducting Indian continental lithosphere (ICL) are still not clear enough to reveal detailed continental collision processes. Seismological methods are the primary ways to obtain images of deep crust and upper-mantle structures. However, previous temporary seismic stations have been unevenly distributed over central Tibet. The Institute of Geology and Geophysics, Chinese Academy of Sciences, has initiated a 2D broadband seismic network in central Tibet across the Bangong–Nujiang suture to fill in gaps among earlier north–south linear profiles for the purpose of detecting the lateral variation of the northern end of the subducting ICL. The health status for each station has been checked at each scheduled service trip. The noise level analysis shows a quiet background in central Tibet, with low cultural noise. Preliminary earthquake locations indicate that they are crustal and broadly distributed rather than only occurring along major faults, suggesting a diffused deformation in the conjugated strike-slip fault zone. Preliminary receiver function analysis shows a complicated crust with significant east–west lateral variations.

Online Material: Table of station parameters of the SANDWICH array.

INTRODUCTION

The Tibetan plateau formed after the collision between the Indian and Eurasian continents at ~50 Ma. Tectonic models for the uplift of Tibet typically involve a uniform, nearly horizontal northward underthrusting of the Indian continental lithosphere (ICL) in southern Tibet (e.g., Ni and Barazangi, 1984). In contrast, Zhao and Morgan (1987) proposed that the Indian crust was injected into the Asian lower crust while the Indian mantle lithosphere detached and continues to subduct beneath the southern Asian lithosphere. Many temporary seismic experiments operated from the Himalayas to northern Tibet over the last two decades to detect the crust and upper-mantle structures and to understand the mountain-building process. Most of these experiments were deployed along a linear profile (Fig. 1). These include the Program for Array Seismic Studies of Continental Lithosphere (PASSCAL91) experiment (Owens *et al.*, 1993), the International Deep Profiling of Tibet and the Himalaya (INDEPTH) II/III project (Kind *et al.*, 1996; Huang *et al.*, 2000), the Himalayan–Tibetan Continental Lithosphere during Mountain Building (Hi-CLIMB) array (Nabelek *et al.*, 2009), the Array Network of Tibetan International Lithospheric Observation and Probe Experiments (ANTILOPE) profile (Zhao *et al.*, 2010), the Rift Study Experiment (RISE) profile (Jin *et al.*, 2009), the TITAN array (Zou *et al.*, 2012), the Tibet-31N profile (Zhang *et al.*, 2013; Chen *et al.*, 2015), and the Gangdese 92° E profile (Shi *et al.*, 2015). There are also several 2D seismic arrays being operated in southern, northeastern, and western Tibet, including the Himalayan Nepal Tibet Seismic Experiment (HIMNT; de la Torre and Sheehan, 2005), Namcha Barwa (Sol *et al.*, 2007), A Seismic Collaborative Experiment of Northern Tibet (ASCENT; Yue *et al.*, 2012), and west Tibet (Razi *et al.*, 2014) projects.

Existing seismic tomographic images based on these projects were interpreted to mean that the upper-mantle structure beneath the southern Tibetan plateau approximately south of the Bangong–Nujiang suture (BNS) is dominated by the subduction of the ICL (e.g., Tilmann *et al.*, 2003; Zhou and Murphy, 2005; Kumar *et al.*, 2006; Li *et al.*, 2008; He *et al.*, 2010; Hung *et al.*, 2010; Zhao *et al.*, 2010, 2014; Jiang *et al.*, 2011; Xu *et al.*, 2011; Ceylan *et al.*, 2012; Liang *et al.*, 2012; Nunn *et al.*, 2014; Zhang *et al.*, 2014, 2015). However, significant east–west lateral variations in the dipping geometry and thickness of the ICL have also been observed (Zhou and Murphy, 2005; Li *et al.*, 2008; Liang *et al.*, 2012; Nunn *et al.*, 2014; Bao *et al.*, 2015).

Because of poor site conditions, such as swampy ground in summer and limited financial and instrumentation support, there is no 2D seismic array being operated in central Tibet. Only lin-

doi: 10.1785/0220150243

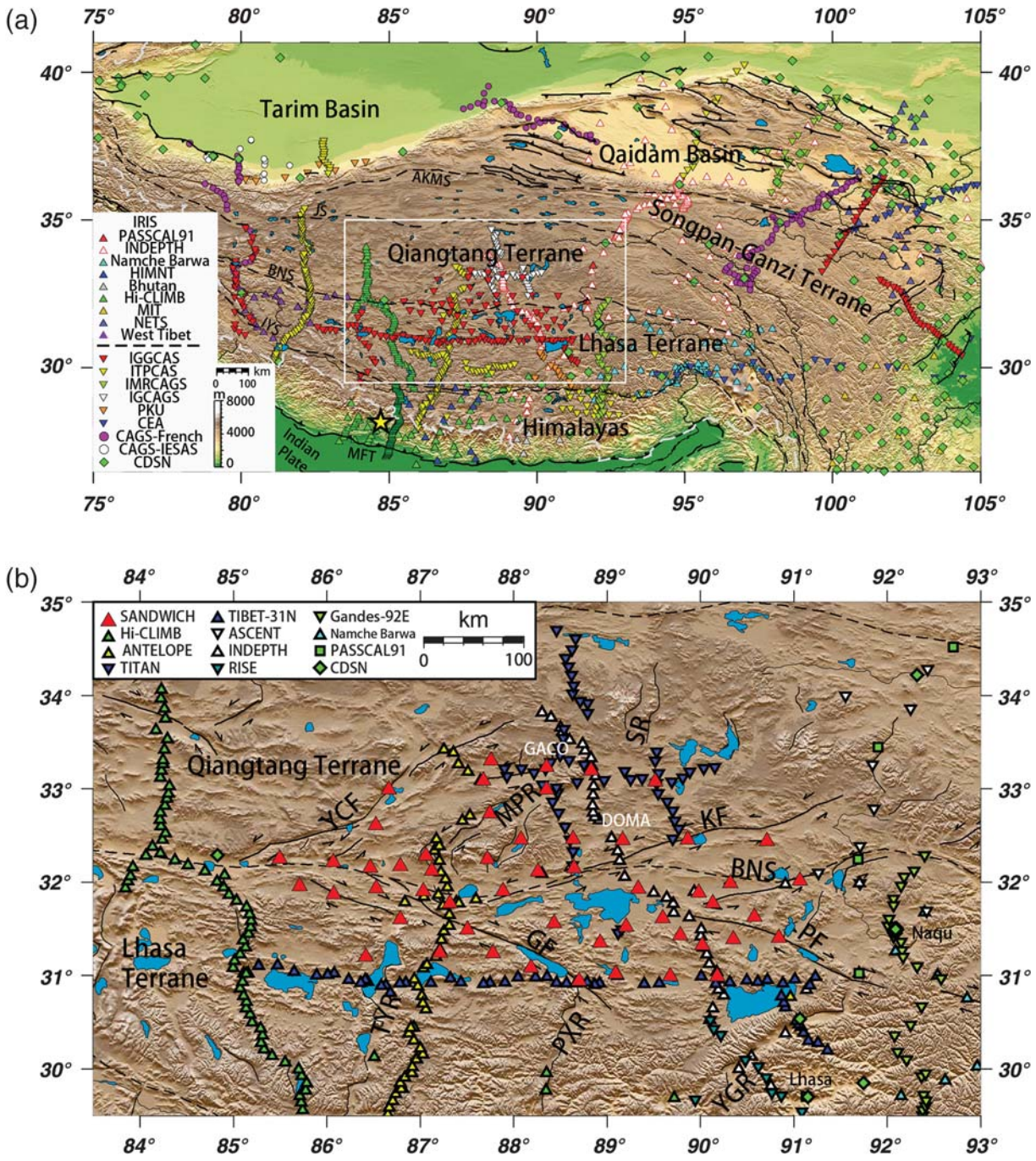

▲ **Figure 1.** Location of the SANDWICH array. (a) Seismic station distribution map in Tibet (incomplete summary by the author). Three kinds of symbols are used for different data source: triangles show Program for Array Seismic Studies of Continental Lithosphere (PASSCAL) experiment stations, with different colors for different experiments; inverted triangles show experiments from different Chinese institutions: Institute of Geology and Geophysics, Chinese Academy of Sciences (IGGCAS), Institute of Tibetan plateau Research, Chinese Academy of Sciences (ITP-CAS), Institute of Mineral Resources, Chinese Academy of Geological Sciences (IMRCAGS), Institute of Geology, Chinese Academy of Geological Sciences (IGCAGS), Peking University (PKU), and the China Earthquake Administration (CEA); circles show two collaborative experiments by CAGS and their collaborators; and diamonds show permanent Chinese Digital Seismic Network (CDSN) stations. Faults and sutures: MFT, Main Frontal fault; IYS, Indus-Yalu suture; BNS, Bangong–Nujiang suture; JS, Jinsha suture; and AKMS, Ayimaqin–Kunlun–Mutztagh suture. (b) Detailed location of the SANDWICH array. Geological structures: BNS, Bangong–Nujiang suture; KF, Kyebxang Co fault; GF, Gyring Co fault; YCF, Yibug–Caka fault; PF, Peng Co fault; TYR, Tangra Yum Co rift; PXR, Pengqu Xianza rift; YGR, Yadong Gulu rift; SR, Shuanghu rift; and MPR, Muga-Puruo rift. Gaco and Doma village stations (GACO and DOMA) are shown on the map and are discussed in Figures 3 and 8, respectively. The epicenter of the 25 April 2015 M_w 7.8 Nepal earthquake is shown as a star; its waveforms are shown in Figure 5. The distance scales for both (a) and (b) are shown based on the scales along 32° N. The color scales of topography for both (a) and (b) are the same and shown in (a).

ear profiles have been deployed up to the central Qiangtang Terrane, and these profiles do not provide good seismic constraints for imaging the northern extent and east–west lateral variation of the ICL perpendicular to the plate convergence direction, because of their limited east–west coverage. It is necessary to deploy a 2D broadband seismic array at central Tibet in order to illuminate the crust and upper mantle of the plateau and to accurately determine the geometry of the northern end of the ICL. This is the primary motivation for our 2D Seismic Array iNtegrated Detection for a Window of Indian Continental Head (SANDWICH) array. This 2D array will help us to obtain a clearer image of the crust and upper-mantle structure in central Tibet with good east–west coverage and to discriminate different tectonic and seismic models of plateau formation.

The most obvious geologic surficial structures in central Tibet are a series of conjugate strike-slip faults distributed from the northern Lhasa terrane to the southern Qiangtang terrane. These strike-slip faults are evenly distributed along both sides of the BNS, forming a right lateral motion between the Lhasa block and the Qiangtang block. All these faults converge toward the BNS; they are left lateral with northeast striking at the north side of the BNS and right lateral with northwest striking at the south side of the BNS (Fig. 1b). There is a series of north–south-trending rifts located to the south and north of this conjugate strike-slip fault zone. These conjugate strike-slip faults are kinematically associated with north–south-trending rifts, regarded as accommodation between coeval east–west extension and north–south contraction of the southern Tibetan plateau (Taylor *et al.*, 2003). Seismicity and focal mechanism analysis for local earthquakes recorded by our SANDWICH array is a good proxy to study the synchronous deformation mechanisms of these strike-slip faults and the small extensional pull-apart basins between the strike-slip fault system. The new data are useful for understanding the overall deformation of the Tibetan plateau.

INSTRUMENT DEPLOYMENT

The SANDWICH seismic array is a 2D broadband seismic array deployed around the BNS in central Tibet, installed by the tectonophysics group of the Tethys Research Center at the Institute of Geology and Geophysics, Chinese Academy of Sciences (IGGCAS). The SANDWICH array began recording in early November 2013 and is expected to finish in November 2017. It consists of 53 intermediate-band seismometers equipped with Güralp CMG-3ESP three-component sensors, with a response band from 60/30 s to 50 Hz, and RefTek 72A-8/130-1 or DAS24-3D 24-bit digital recorders (see Ⓔ Table S1, available in the electronic supplement to this article). The data are recorded in three components with a sampling rate of 40 samples/s. All instruments are powered by 12 V deep-cycle lead-acid batteries charged by two 60 W solar panels (Fig. 2b). Sensors are seated on a granite pad fixed by plaster at the bottom of a 1-m-depth vault, surrounded by thermally insulated foam in a plastic barrel, and covered by excavated soil (Fig. 2c). The stations are distributed on both sides of the BNS, from the northern Lhasa terrane to the southern Qiangtang terrane (Fig. 1), and station spacing is approximately 40 km on average. With this finer station spacing, we expect to have a good control for the location of local seismicity and to obtain a high-resolution image of the crustal and upper-mantle structure beneath central Tibet.

OVERALL DATA QUALITY

There have been more than 300 GB of data accumulated since the deployment of the instruments. We have monitored the status of health (SOH) of all the instruments and replaced hardware parts with bad status, such as flooded sensors and recorders, broken Global Positioning System (GPS) antennas (Fig. 2a) and solar panels to keep all the stations working during their service.

The noise level of every component at each station is checked by computing the power spectral density (PSD) and the corresponding probability density functions (PDFs). Noise PSDs/PDFs can directly reflect the SOH of the instruments and their corresponding data quality. We selected two 1-hr-length waveforms from the continuous record of each day; waveforms were from 2:00 to 3:00 p.m. and from 2:00 to 3:00 a.m. local time (GMT+8:00). These time slots are representative of both daylight working time and quiet night time. Noise PSDs are calculated using Robert Herrmann's PSD calculation instructions (see Data and Resources). The PDFs of these PSDs are then calculated using the Incorporated Research Institutions for Seismology (IRIS) Noise Toolkit PDF–PSD (see Data and Resources).

The noise level of the vertical components is quite low for all the stations. An example of the PDFs is shown for the GACO station in Figure 3 (for the location of GACO, see Fig. 1b). The noise level during daylight working time shows more high-frequency noise than the noise level at quiet night time. This result reflects the high-frequency noise of human activity around the shallow-seated sensors during the day. The noise level of low frequency (lower than 2 s) is quite similar for both daylight working time and quiet night time. This result shows that cultural noise generated by human activities is mainly high-frequency noise. Horizontal components show stronger noise for both high- and low-frequency bands than the vertical component (Fig. 3). The overall noise level for the three components is reasonably low for the temporary stations when compared with noise models based on global permanent station observations (Peterson, 1993). These low noise levels are reflected in the clean sample waveforms (Figs. 4–6).

INITIAL OBSERVATIONS

Figures 4, 5, and 6, respectively, show waveform examples for one teleseismic event, two regional events, and one local event recorded by the SANDWICH array. These waveform examples show the ability of the network to record high signal-to-noise ratio (SNR) seismic waveforms because of the low background noise level. The teleseismic event shows good SNR for all major phases. The teleseismic signals are useful for shear-wave splitting measurements, receiver function analysis, teleseismic body-wave travel-time tomography, and surface-wave tomography (Fig. 4). Raw vertical-component waveforms show the source

▲ **Figure 2.** Field deployment of a station. (a) Overlook of station QANM, located at the northeastern corner of a Tibetan house, when we were testing a Global Positioning System (GPS) antenna because of the bad status of health for its GPS clock, shown by the overlain phase error curve at the bottom of (a), in which the dashed line means no GPS phase information. (b) Setup details for a station (WQAM), including solar panels, GPS antenna, and buried sensor and recorder. (c) Deployment of a sensor in the field. The sensor is seated on a granite pad fixed by plaster at the bottom of a 1-m-depth vault.

rupture features of the Nepal M_w 7.8 earthquake. This information is useful for the inversion of source rupture processes and regional structures (Fig. 5a). The epicenter of the Nepal earthquake occurred relatively close to the array. The close proximity of the earthquake and the strong ground motion it generated caused the surface waves to clip when they exceeded the dynamic range of the sensor. The clear *Pn* phases and the first arrival transition from *Pg* to *Pn* phases could be observed on the waveforms of local–regional earthquakes (Fig. 5b). The lower magnitude limit of our sensors is M_L 1.6 according to our preliminary location results for local events (see Preliminary Results section). The waveforms of an

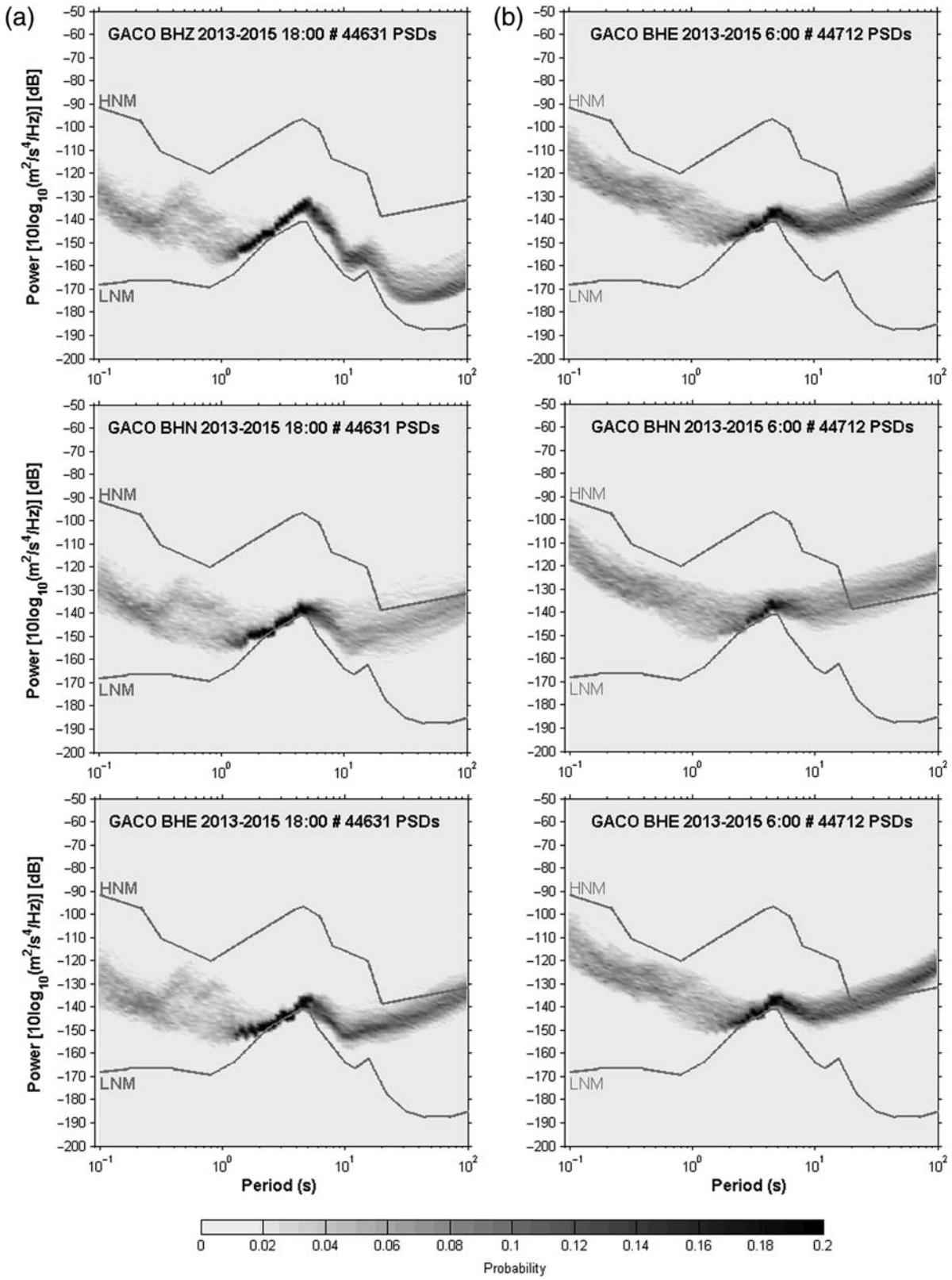

▲ **Figure 3.** Noise probability density functions (PDFs) of GACO station during the daytime and night. (a) Noise PDF for a 1-hr-long three-component waveform between 2:00 p.m. and 3:00 p.m. (6:00–7:00 GMT) of each day for GACO station. (b) Noise PDF for a 1-hr-long three-component waveform between 2:00 a.m. and 3:00 a.m. (18:00–19:00 GMT) of each day for GACO station.

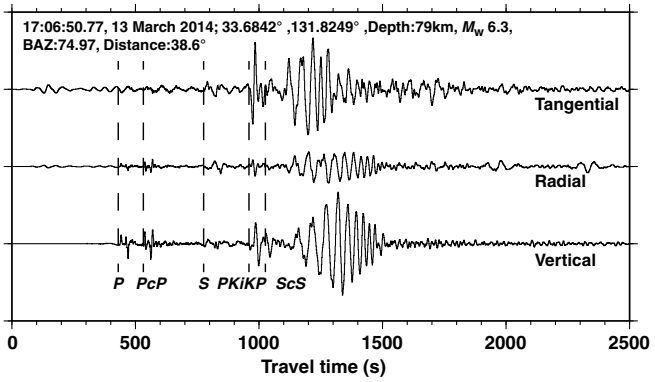

▲ **Figure 4.** Example data of a teleseismic event. The information for the earthquake is shown on top of the waveforms. Several major phases are labeled on the plot, based on travel times from the 1991 International Association of Seismology and Physics of the Earth's Interior (IASP91) model.

M_L 1.6 local earthquake from our preliminary location results show very good SNR at short-distance stations for all three components (Fig. 6). Local and regional earthquake signals could be used to analyze the regional stress scheme and active seismogenic structures and to conduct body-wave travel-time and attenuation tomography.

PRELIMINARY RESULTS

Because the array has been deployed for more than a year, the accumulated data are good enough to perform many seismic analyses, including local seismicity analysis, receiver function analysis, ambient noise tomography, shear-wave splitting, and teleseismic body-wave tomography. These preliminary results have given us useful information about the Earth's structure from the upper crust to the upper mantle underneath central Tibet. The ultimate target of this project is to integrate all of these seismic results to obtain a comprehensive image of the crustal and upper-mantle structure of central Tibet.

Preliminary results from local seismicity analysis and receiver functions are shown in the following sections. Detailed results will be finalized after the conclusion of the field deployment and subsequently report significant findings to the community.

Local Seismicity Analysis

Because of the lack of permanent seismic stations in central Tibet (Fig. 1), regional catalogs could not provide a reliable location for small earthquakes. Thus, an event-detection algorithm (Langin *et al.*, 2003; Liang *et al.*, 2008) based on the ratio of an averaged short-term amplitude (STA) to an averaged long-term amplitude (LTA) was used to identify local events. To avoid potential time shifts on phases caused by filtering effects, original waveforms were used for most of the phase picks, with the exception of a few noisy data. In these cases, a 0.5–5 Hz band-pass filter was applied. We then used HYPOINVERSE-2000 (Klein, 2002) to locate these selected events. A 1D velocity model from CRUST1.0 (Laske *et al.*, 2013) was used in our analysis of the locations.

A total of 233 local events have been located with magnitudes ranging from M_L 1.6 to 5.3 in the vicinity of the SANDWICH array (any STA/LTA ratio values greater than 3.5 and measured by at least 13 stations were kept). The distribution of these events could be separated into two groups based on their relations with local geologic structures (Fig. 7). Events in the first group, moderate-size earthquakes with magnitudes larger than M_L 5.0, are well correlated with known normal and strike-slip faults in the region. Several clusters occur along many of the normal faults, whereas many other earthquakes are sparsely distributed along the northeast-trending Yibug Caka fault zone north of the BNS and the northwest-trending Gyaring Co fault zone south of the BNS. At the same time as the second group, many events do not show clear correlations with the known structures that occur between the conjugate strike-slip faults. Both our observations and the event distribution from the International Seismological Centre catalog imply that the strain energy released in central Tibet is mainly by normal and strike-slip movements along major faults. However, there is also a significant component of diffused energy release on minor faults in the conjugate strike-slip fault zone. This observation suggests that continuous or diffused deformation of the Tibetan upper crust, or perhaps the whole lithosphere, is occurring. The possibility of continuous or diffused deformation has been suggested based on prior GPS observations (Zhang *et al.*, 2004).

Receiver Function Analysis

We adopt a method of time-domain deconvolution (Ammon, 1991) to calculate the receiver functions of every station. We used a window of 120 s (20 s before and 100 s after the *P* arrival) to select waveforms and calculate receiver functions. The receiver functions of station DOMA from one and a half years worth of data are shown in Figure 8. The Moho *Ps* converted phase is at ~8.5 s. After preliminary $H-\kappa$ analysis, the determined Moho depth will be ~63 km and the corresponding V_P/V_S ratio is ~1.81, using an averaged *P*-wave crustal velocity $V_P = 6.3$ km/s (Fig. 8, left). We can see azimuthal variations for the Moho *Ps* converted phases and other intracrust converted phases. The azimuthal coverage of the data for the southwest quadrant is relatively poor because there were no satisfactory earthquakes from the African continent, southwest Indian Ocean, or Atlantic Ocean. The low SNR of multiple converted phases makes the classic $H-\kappa$ stacking results unstable (Zhu and Kanamori, 2000), which might be caused by complicated crustal structure beneath the station, including an inclining velocity boundary or an anisotropic layer in the crust.

SUMMARY

The temporary seismic network SANDWICH has been deployed to record both local and teleseismic waveforms for studying the crustal and upper-mantle structure in central Tibet. There are 53 broadband stations covering both sides of the BNS from the northern Lhasa terrane to the southern Qiangtang terrane be-

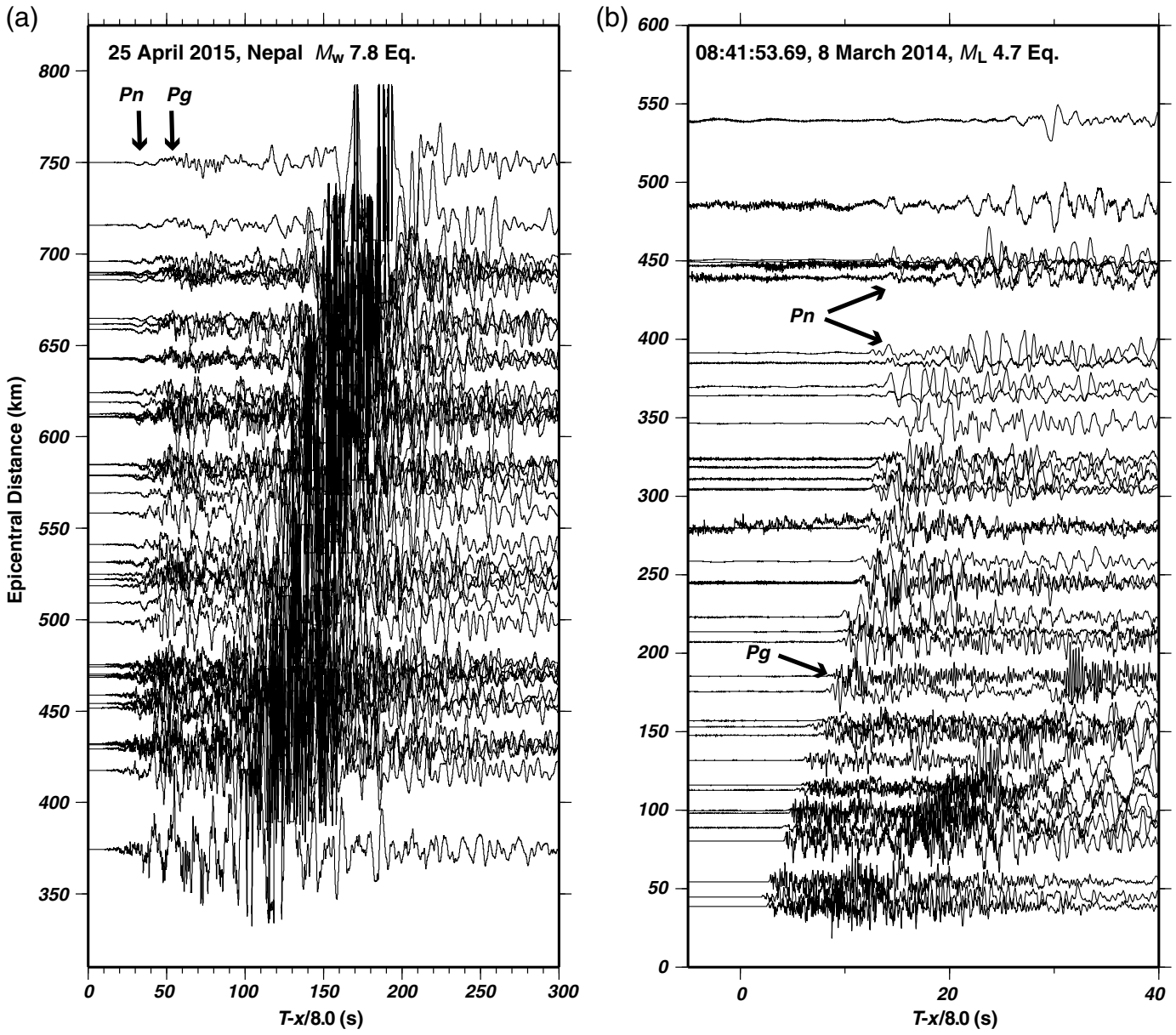

▲ **Figure 5.** Example vertical-component waveforms of two local (regional) earthquakes. (a) Waveforms with reduced travel time for the 25 April 2015 M_w 7.8 Nepal earthquake. Because the SANDWICH array is close to the epicenter, the strong surface waves are clipped on the records. (b) Waveform with reduced travel time for an M_L 4.7 earthquake located to the east of SANDWICH array. The location of the earthquake is shown in Figure 7.

tween 85° E and 91° E. This network significantly improves the station coverage of central Tibet. This project has provided us a chance to investigate strike-slip and normal faulting in central Tibet, as well as the lateral variation of the northern extent of the ICL, and to understand the transition from a significant east–west extension in southern Tibet to conjugate strike-slip faulting in central and northern Tibet.

DATA AND RESOURCES

The project is expected to be complete in November 2017. The expected total volume of original waveform and metadata is ~750 GB. The data will be analyzed by the tectonophysics group of the Tethys Research Center at Institute of Geology and Geophysics, Chinese Academy of Sciences (IGGCAS). Any collaborative work that could fully extend the usage of this dataset is welcome at the current stage, and any scientists who wish to work together with us on this dataset are encouraged to contact Xiaobo Tian (txb@mail.iggcas.ac.cn) and Xiaofeng Liang (liangxf@mail.iggcas.ac.cn). Our data will be submitted to the data center of the Seismic Array Laboratory, IGGCAS (http://www.seislab.cn/data/). The data center is currently working on a collaborative open mechanism with the Incorporated Research Institutions for Seismology (IRIS) Data Management Center to

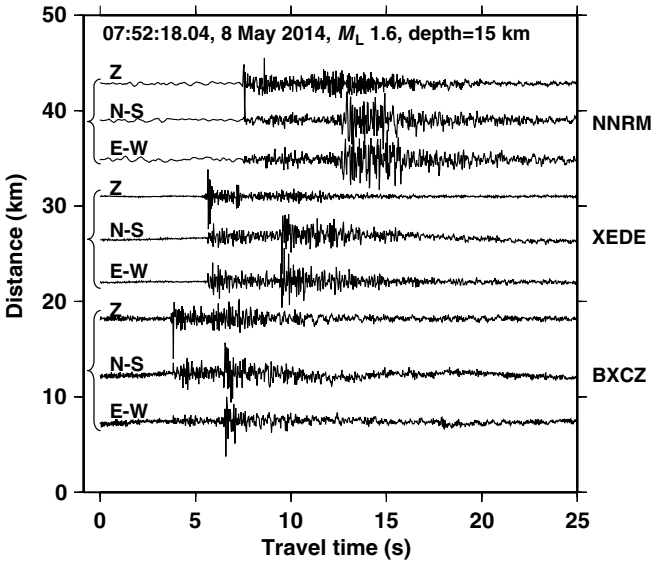

▲ **Figure 6.** Three-component waveforms from the three stations closest to a local M_L 1.6 earthquake. Location of this earthquake and the corresponding stations are shown in Figure 7.

share the data with the public and to provide easier access. The network code 6A (2013–2016) has been assigned to the SANDWICH array by the International Federation of Digital Seismograph Networks (FDSN).

Noise power spectral densities (PSDs) are calculated using Robert Herrmann's PSD calculation instructions (http://www.eas.slu.edu/eqc/eqc_cps/SACPSD/SACPSD.tgz, last accessed August 2015). The PDFs of these PSDs are then calculated using the Incorporated Research Institutions for Seismology (IRIS) Noise Toolkit PDF–PSD (http://ds.iris.edu/ds/products/noise-toolkit-pdf-psd/, last accessed August 2015). The Generic Mapping Tools (GMT) and pssac codes (written by Lupei Zhu of St. Louis Univeristy, http://www.eas.slu.edu/People/LZhu/downloads/pssac.c, last accessed August 2015) were used to produce the figures. Seismic Analysis Code (SAC) was used for data processing.

ACKNOWLEDGMENTS

We would like to express our appreciation to Zhongjie Zhang, who passed away suddenly on 6 September 2013. Without his efforts, the SANDWICH project would not have begun. We thank our colleagues at our institution and our Tibetan drivers for their

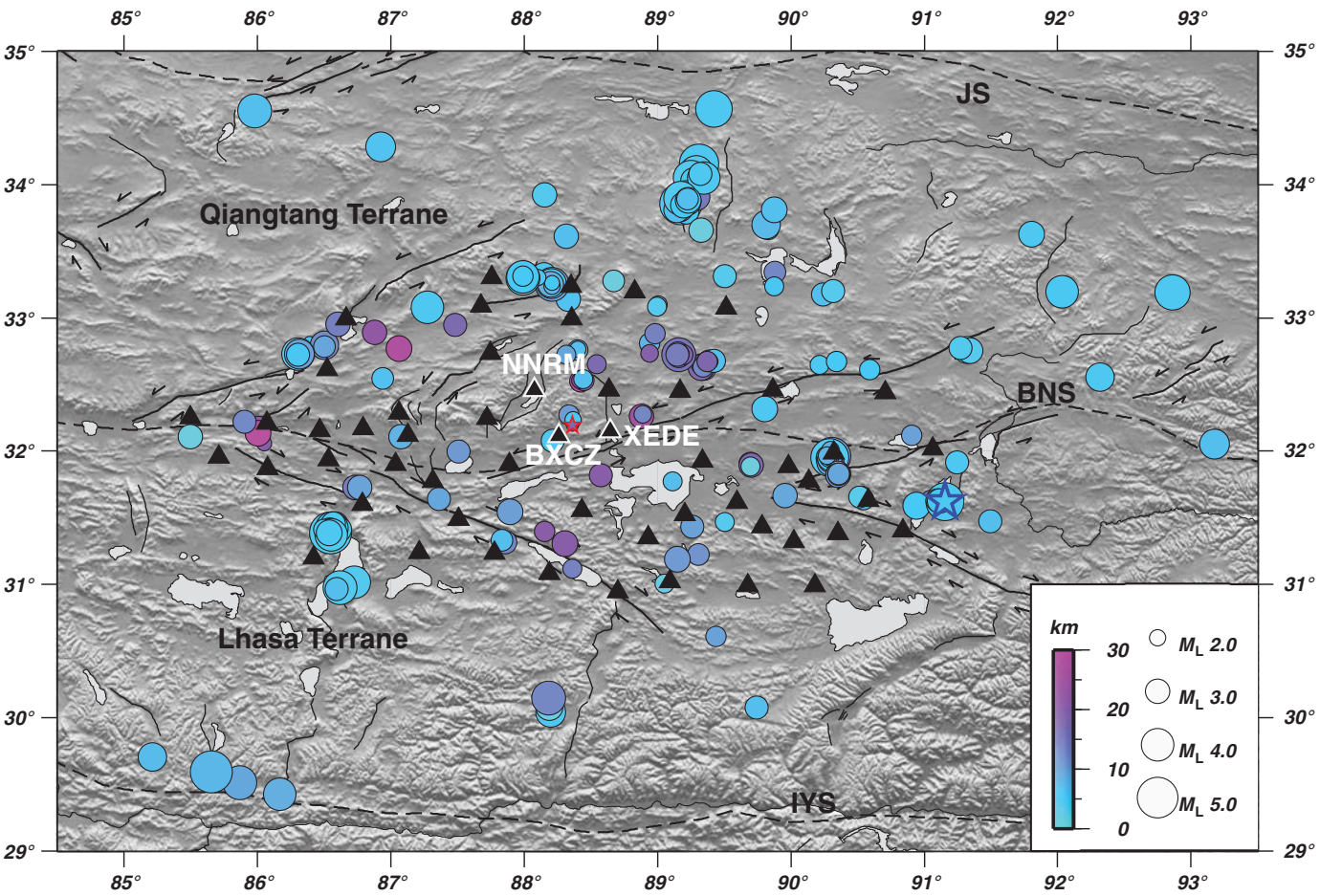

▲ **Figure 7.** Preliminary results for local seismicity location. Circles of different sizes represent the local magnitudes of each earthquake, and focal depths are color coded. Triangles with white edges show the stations used to locate the M_L 1.6 earthquake (red star) in Figure 6. The blue star shows the location of the M_L 4.7 earthquake shown in Figure 5.

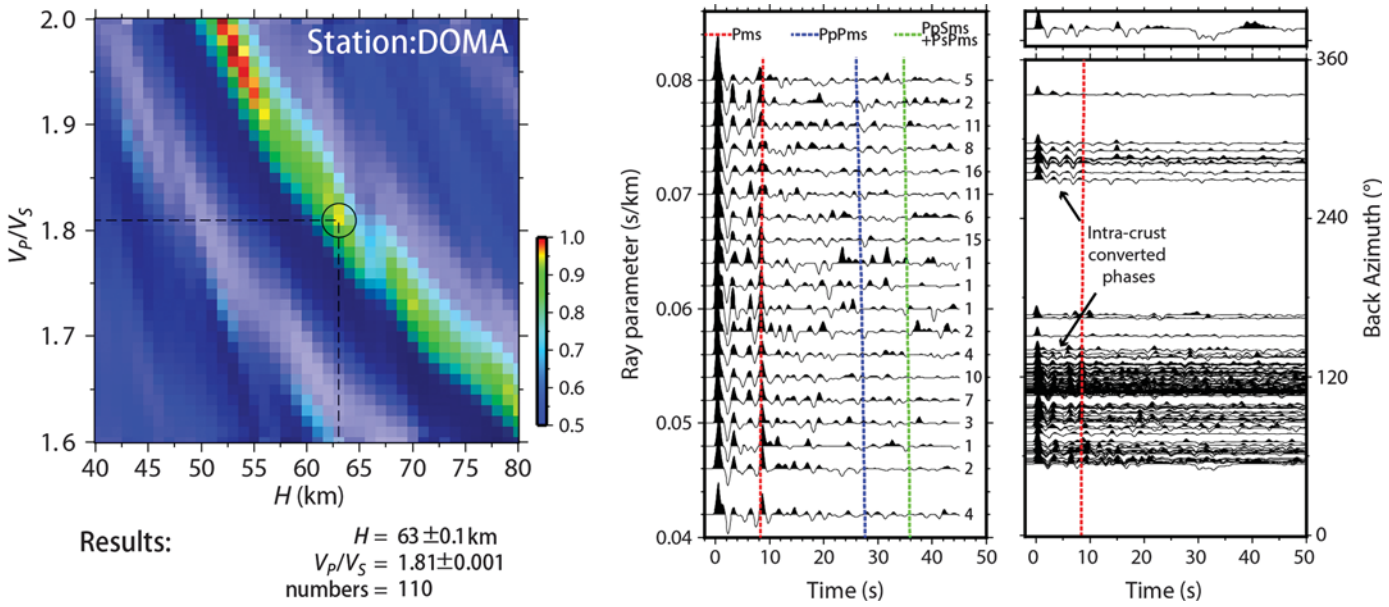

▲ **Figure 8.** Preliminary receiver function analysis results for DOMA station. (left) $H-\kappa$ analysis results. (center) The stacked receiver functions with different ray parameters. The numbers at right of the waveforms are the number of receiver functions to generate the stacked waveforms. (right) panel The receiver functions aligning with different back azimuth; the stack trace of all receiver functions is shown at the top.

help in the field. We thank the Seismic Array Laboratory, Institute of Geology and Geophysics, Chinese Academy of Sciences (IGGCAS), who provided the instruments and maintenance services for the SANDWICH experiment. Qi-Fu Chen has provided helpful suggestions for the seismicity analysis. James Ni and Andrea Gallegos kindly helped to improve the manuscript. Constructive comments from Zhigang Peng, the associated editor, and two anonymous reviewers also helped to improve the manuscript. Locations of permanent station (CDSN) for this study are provided by Data Management Centre of China National Seismic Network at Institute of Geophysics, China Earthquake Administration (SEISDMC, doi 10.7914/SN/CB). We also acknowledge Robert Herrmann and the Incorporated Research Institutions for Seismology (IRIS) Data Service for making the power spectral density and probability density function calculation codes available. The SANDWICH project is supported by the Strategic Priority Research Program (B) of the Chinese Academy of Sciences (Grant XDB03010700) and the National Natural Science Foundation of China Grants 41404051, 41274066, 41374063, 41274090, and 41574056.

REFERENCES

Ammon, C. J. (1991). The isolation of receiver effects from teleseismic *P* waveforms, *Bull. Seismol. Soc. Am.* **81,** no. 6, 2504–2510.

Bao, X., X. Song, and J. Li (2015). High-resolution lithospheric structure beneath mainland China from ambient noise and earthquake surface-wave tomography, *Earth Planet. Sci. Lett.* **417,** 132–141, doi: 10.1016/j.epsl.2015.02.024.

Ceylan, S., J. Ni, J. Y. Chen, Q. Zhang, F. Tilmann, and E. Sandvol (2012). Fragmented Indian plate and vertically coherent deformation beneath eastern Tibet, *J. Geophys. Res.* **117,** no. B11, B11303, doi: 10.1029/2012JB009210.

Chen, Y., W. Li, X. Yuan, J. Badal, and J. Teng (2015). Tearing of the Indian lithospheric slab beneath southern Tibet revealed by *SKS*-wave splitting measurements, *Earth Planet. Sci. Lett.* **413,** 13–24, doi: 10.1016/j.epsl.2014.12.041.

de la Torre, T., and A. Sheehan (2005). Broadband seismic noise analysis of the Himalayan Nepal Tibet seismic experiment, *Bull. Seismol. Soc. Am.* **95,** 1202–1208.

He, R., D. Zhao, R. Gao, and H. Zheng (2010). Tracing the Indian lithospheric mantle beneath central Tibetan plateau using teleseismic tomography, *Tectonophysics* **491,** nos. 1/4, 230–243.

Huang, W. C., J. F. Ni, F. Tilmann, D. Nelson, J. Guo, W. Zhao, J. Mechie, R. Kind, J. Saul, R. Rapine, and T. M. Hearn (2000). Seismic polarization anisotropy beneath the central Tibetan plateau, *J. Geophys. Res.* **105,** no. B12, 27,979–27,989.

Hung, S.-H., W.-P. Chen, L.-Y. Chiao, and T.-L. Tseng (2010). First multi-scale, finite-frequency tomography illuminates 3-D anatomy of the Tibetan plateau, *Geophys. Res. Lett.* **37,** no. 6, 1–5.

Jiang, M., S. Zhou, E. Sandvol, X. Chen, X. Liang, Y. J. Chen, and W. Fan (2011). 3-D lithospheric structure beneath southern Tibet from Rayleigh-wave tomography with a 2-D seismic array, *Geophys. J. Int.* **185,** no. 2, 593–608, doi: 10.1111/j.1365-246X.2011.04979.x.

Jin, G., Y. Chen, and C. Basang (2009). Investigation of local earthquakes in the Lhasa region, *Chin. J. Geophys.* **52,** no. 12, 3020–3026, doi: 10.3969/j.issn.0001-5733.2009.12.011.

Kind, R., J. Ni, W. Zhao, J. Wu, X. Yuan, L. Zhao, E. Sandvol, C. Reese, J. Nabelek, and T. Hearn (1996). Evidence from earthquake data for a partially molten crustal layer in southern Tibet, *Science* **274,** 1692–1694.

Klein, F. W. (2002). User's Guide to HYPOINVERSE-2000, a Fortran program to solve for earthquake locations and magnitudes, *U.S. Geol. Surv. Open-File Rept. 02-171*.

Kumar, P., X. Yuan, R. Kind, and J. Ni (2006). Imaging the colliding Indian and Asian lithospheric plates beneath Tibet, *J. Geophys. Res.* **111,** no. B6, B06308, doi: 10.1029/2005jb003930.

Langin, W. R., L. D. Brown, and E. A. Sandvol (2003). Seismicity of central Tibet from Project INDEPTH III seismic recordings, *Bull. Seismol. Soc. Am.* **93,** 2146–2159.

Laske, G., G. Masters, Z. Ma, and M. Pasyanos (2013). Update on CRUST1.0–A 1-degree global model of Earth's crust, *Geophys. Res. Abstr.* **15,** EGU2013–2658.

Li, C., R. D. van der Hilst, A. S. Meltzer, and E. R. Engdahl (2008). Subduction of the Indian lithosphere beneath the Tibetan plateau and Burma, *Earth Planet. Sci. Lett.* **274,** 157–168.

Liang, X., E. Sandvol, Y. J. Chen, T. Hearn, J. Ni, S. Klemperer, Y. Shen, and F. Tilmann (2012). A complex Tibetan upper mantle: A fragmented Indian slab and no south-verging subduction of Eurasian lithosphere, *Earth Planet. Sci. Lett.* **333/334,** 101–111, doi: 10.1016/j.epsl.2012.03.036.

Liang, X., S. Zhou, Y. J. Chen, G. Jin, L. Xiao, P. Liu, Y. Fu, Y. Tang, X. Lou, and J. Ning (2008). Earthquake distribution in southern Tibet and its tectonic implications, *J. Geophys. Res.* **113,** no. B12, B12409, doi: 10.1029/2007JB005101.

Nabelek, J., G. Hetenyi, J. Vergne, S. Sapkota, B. Kafle, M. Jiang, H. P. Su, J. Chen, B. S. Huang, and H.-C. Team (2009). Underplating in the Himalaya–Tibet collision zone revealed by the Hi-CLIMB experiment, *Science* **325,** no. 5946, 1371–1374, doi: 10.1126/science.1167719.

Ni, J., and M. Barazangi (1984). Seismotectonics of the Himalayan collision zone D geometry of the underthrusting Indian plate beneath the Himalaya, *J. Geophys. Res.* **89,** 1147–1163.

Nunn, C., S. W. Roecker, K. F. Priestley, X. Liang, and A. Gilligan (2014). Joint inversion of surface waves and teleseismic body waves across the Tibetan collision zone: The fate of subducted Indian lithosphere, *Geophys. J. Int.* **198,** no. 3, 1526–1542, doi: 10.1093/gji/ggu193.

Owens, T. J., G. E. Randall, F. T. Wu, and R. Zeng (1993). PASSCAL instrument performance during the Tibetan plateau passive seismic experiment, *Bull. Seismol. Soc. Am.* **83,** 1959–1970.

Peterson, J. (1993). Observation and modeling of seismic background noise, *U.S. Geol. Surv. Open-File Rept. 93–322.*

Razi, A. S., V. Levin, S. W. Roecker, and G.-C. D. Huang (2014). Crustal and uppermost mantle structure beneath western Tibet using seismic traveltime tomography, *Geochem. Geophys. Geosyst.* **15,** no. 2, 434–452, doi: 10.1002/2013GC005143.

Shi, D., Z. Wu, S. L. Klemperer, W. Zhao, G. Xue, and H. Su (2015). Receiver function imaging of crustal suture, steep subduction, and mantle wedge in the eastern India–Tibet continental collision zone, *Earth Planet. Sci. Lett.* **414,** 6–15, doi: 10.1016/j.epsl.2014.12.055.

Sol, S., A. Meltzer, R. Burgmann, R. D. van der Hilst, R. King, Z. Chen, P. O. Koons, E. Lev, Y. P. Liu, P. K. Zeitler, *et al.* (2007). Geodynamics of the southern Tibetan plateau from seismic anisotropy and geodesy, *Geology* **35,** 563–566.

Taylor, M., A. Yin, F. J. Ryerson, P. Kapp, and L. Ding (2003). Conjugate strike-slip faulting along the Bangong–Nujiang suture zone accommodates coeval east–west extension and north–south shortening in the interior of the Tibetan plateau, *Tectonics* **22,** no. 4, 1044, doi: 10.1029/2002tc001361.

Tilmann, F., J. Ni, and INDEPTH Seismic Team (2003). Seismic imaging of the downwelling Indian lithosphere beneath central Tibet, *Science* **300,** 1424–1427.

Xu, Q., J. Zhao, S. Pei, and H. Liu (2011). The lithosphere–asthenosphere boundary revealed by *S*-receiver functions from the Hi-CLIMB experiment, *Geophys. J. Int.* **187,** no. 1, 414–420, doi: 10.1111/j.1365-246X.2011.05154.x.

Yue, H., Y. J. Chen, E. Sandvol, J. Ni, T. Hearn, S. Zhou, Y. Feng, Z. Ge, A. Trujillo, Y. Wang, *et al.* (2012). Lithospheric and upper mantle structure of the northeastern Tibetan plateau, *J. Geophys. Res.* **117,** no. B5, B05307, doi: 10.1029/2011JB008545.

Zhang, H., D. Zhao, J. Zhao, and H. Liu (2015). Tomographic imaging of the underthrusting Indian slab and mantle upwelling beneath central Tibet, *Gondwana Res.* **28,** no. 1, 121–132, doi: 10.1016/j.gr.2014.02.012.

Zhang, P. Z., Z. Shen, M. Wang, W. Gan, R. Burgmann, P. Molnar, Q. Wang, Z. Niu, J. Sun, J. Wu, *et al.* (2004). Continuous deformation of the Tibetan plateau from global positioning system data, *Geology* **32,** 809–812.

Zhang, X., J. Teng, R. Sun, F. Romanelli, Z. Zhang, and G. F. Panza (2014). Structural model of the lithosphere–asthenosphere system beneath the Qinghai–Tibet plateau and its adjacent areas, *Tectonophysics* **634,** 208–226, doi: 10.1016/j.tecto.2014.08.017.

Zhang, Z., Y. Chen, X. Yuan, X. Tian, S. L. Klemperer, T. Xu, Z. Bai, H. Zhang, J. Wu, and J. Teng (2013). Normal faulting from simple shear rifting in south Tibet, using evidence from passive seismic profiling across the Yadong-Gulu rift, *Tectonophysics* **606,** 178–186, doi: 10.1016/j.tecto.2013.03.019.

Zhao, J., X. Yuan, H. Liu, P. Kumar, S. Pei, R. Kind, Z. Zhang, J. Teng, L. Ding, X. Gao, Q. Xu, and W. Wang (2010). The boundary between the Indian and Asian tectonic plates below Tibet, *Proc. Natl. Acad. Sci. Unit. States Am.* **107,** no. 25, 11,229–11,233, doi: 10.1073/pnas.1001921107.

Zhao, J., D. Zhao, H. Zhang, H. Liu, Y. Huang, H. Cheng, and W. Wang (2014). *P*-wave tomography and dynamics of the crust and upper mantle beneath western Tibet, *Gondwana Res.* **25,** no. 4, 1690–1699, doi: 10.1016/j.gr.2013.06.020.

Zhao, W.-L., and W. J. Morgan (1987). Injection of Indian crust into Tibetan lower crust: A two-dimensional finite element model study, *Tectonics* **6,** no. 4, 489–504, doi: 10.1029/TC006i004p00489.

Zhou, H. W., and M. A. Murphy (2005). Tomographic evidence for wholesale underthrusting of India beneath the entire Tibetan plateau, *J. Asian Earth Sci.* **25,** 445–457.

Zhu, L. P., and H. Kanamori (2000). Moho depth variation in southern California from teleseismic receiver functions, *J. Geophys. Res.* **105,** no. B2, 2969–2980.

Zou, C., R. He, R. Gao, Z. Zhang, and H. Zheng (2012). Deep structure of the central uplift belt in the Qiangtang terrane Tibetan plateau from teleseismic *P*-wave tomography, *Chin. Sci. Bull.* **57,** nos. 28/29, 2729–2739 (in Chinese).

Xiaofeng Liang
Xiaobo Tian[1]
Gaohua Zhu[2]
Chenglong Wu[2]
Yaohui Duan[2]
Wei Li[2]
Beibei Zhou[2]
Minghui Zhang[2]
Guiping Yu[2]
Shitan Nie[2]
Gaochun Wang[2]
Minling Wang
Zhenbo Wu[2]
Zhen Liu
Xi Guo[2]
Xiaopeng Zhou[2]
Zhi Wei[2]
Tao Xu[1]
Xi Zhang
Zhiming Bai
Yun Chen
Jiwen Teng
State Key Laboratory of Lithospheric Evolution
Institute of Geology and Geophysics
Chinese Academy of Sciences (CAS)
No. 19 Beitucheng West Road, Chaoyang
Beijing 100029, China
liangxf@mail.iggcas.ac.cn

Published Online 4 May 2016

[1] Also at CAS Center for Excellence in Tibetan Plateau Earth Sciences, Beijing 100101, China.

[2] Also at University of Chinese Academy of Sciences, Beijing 100049, China.